Eur. Phys. J. D (2022) 76:121
https://doi.org/10.1140/epjd/s10053-022-00448-w

THE EUROPEAN PHYSICAL JOURNAL D

Regular Article – Atomic Physics

Positronium microwave spectroscopy using Ramsey interferometry

T. J. Babij[a] and D. B. Cassidy

Department of Physics and Astronomy, University College London, Gower Street, London, WC1E 6BT, UK

Received 30 March 2022 / Accepted 24 June 2022 / Published online 11 July 2022

Abstract. We describe an experimental arrangement suitable for performing microwave spectroscopy measurements of the positronium (Ps) $n = 2$ fine structure using Ramsey interferometry. Simulations are presented concerning the production of energetic $2\,^3S_1$ Ps atoms from a Xe gas cell, and their subsequent interactions with a pair of waveguides in which coherent microwave radiation fields are applied. We conclude that for realistic experimental parameters, optimized using a Monte Carlo simulation, a gas cell length of 10 cm with a gas pressure of 0.5 Pa and a positron beam energy of 40 eV, count rates on the order of 50 Hz should be possible.

1 Introduction

Because positronium (Ps) [1] has no nuclear structure [2] it is expected to be described by QED theory to extremely high precision [3], with weak force contributions occurring at the part per trillion level [4]. As a result Ps can, in principle, be used to search for 'new physics" [5], since any confirmed deviation of Ps properties from QED would necessarily involve physical mechanisms not included in that theory [6]. Such investigations are only possible, however, if Ps measurements can be performed with a precision comparable to that of the corresponding calculations. Unfortunately Ps experiments are in general far less precise than theory.

QED calculations of Ps energy levels are complete up to order $\mathcal{O}(m\alpha^6)$ (e.g., [7,8]), and work on the higher-order terms is ongoing (e.g., [9]). For the $n = 2$ fine structure intervals, the uncertainty in theory, obtained from estimates of the magnitudes of uncalculated terms, is 80 kHz [10]. Until recently, the experimental uncertainties of these intervals were on the several MHz scale [11–13].

Recently, new measurements of the Ps $n = 2$ fine structure $2\,^3S_1 \rightarrow 2\,^3P_J$ $(J = 0, 1, 2)$ have been performed [14,15]. For these measurements, a positron trap was used to generate a pulsed positron beam [16] which was implanted into a mesoporous silica film to generate a pulsed Ps gas [17]. Excited state Ps atoms were then obtained using laser excitation [18]. This approach is more efficient than the previous methods [19], and also results in the creation of slower atoms, with typical energies of around 50 meV [20]. This means that Ps atoms passing through waveguides (whose size is dictated by the frequency of the radiation used) experience less transit-time broadening, and that lower power microwave radiation can be employed, reducing power broadening effects (e.g., [21]), and thus resulting in narrower lineshapes.

These advances allowed sub-MHz precision to be obtained, with limitations arising primarily from statistical uncertainties. However, despite the improved precision, a disagreement with theory was observed [14], as well as asymmetries in some of the measured lineshapes [15], suggesting the presence of unknown systematic effects. Subsequent numerical simulations of the experimental apparatus have indicated that reflections of microwave radiation in the vacuum chamber back into the waveguides may have been responsible for the observed asymmetries [22].

An intrinsic limitation of direct spectroscopic measurements of the Ps $n = 2$ fine structure is that the transitions have a natural linewidth of 50 MHz, determined by the 3.19 ns radiative lifetime of the $2\,^3P_J$ levels. In order for experiments to reach a level of precision commensurate with the 80 kHz theory uncertainties, the 50 MHz line must be split by approximately 1000. While this is certainly possible (for example Beyer and co-workers have obtained measurements with a precision corresponding to one part in 10,000 of the 20 MHz linewidth in one-photon 2S-4P transitions in hydrogen [23]), it requires a complete understanding of the lineshape; even small effects that distort such broad lineshapes can result in large uncertainties in the inferred transition frequencies.

As discussed in more detail in Sect. 4, this problem can be mitigated using the Ramsey technique of separated oscillatory fields (SOF) [24]. The SOF method addresses the linewidth problem because it allows one to effectively obtain narrower linewidths by replacing

[a] e-mail: t.babij@ucl.ac.uk (corresponding author)

the single interaction region with a pair of (coherent) microwave radiation fields, separated by some distance D. Atoms are excited to a superposition state in one field, and then pass with speed v through the field-free region for a time $T = D/v_{\rm Ps}$. The second interaction returns the atoms to the initial state, yielding an interference effect that narrows the line by a factor of two, even for $T = 0$. For $T > 0$ the linewidth is further narrowed, and depends on T, rather than the Ps lifetime (essentially, by selecting longer-lived atoms). The price of this advantage is loss of signal; the loss fraction depends on the particular superposition state populations, but for lifetimes close to 3.2 ns, a factor of 5 linewidth reduction (i.e., $T = 16$ ns), would incur a signal loss of two orders of magnitude. This highlights why standard Ps production methods [19] cannot be used for SOF measurements: 50 meV Ps atoms have a speed $v_{\rm Ps} = 9 \times 10^6$ cm/s, which would travel only 0.14 cm in 16 ns. Since this is much less than the $\approx$ cm dimensions of the relevant waveguides used for the fine structure measurements [15], a SOF signal cannot be obtained using such slow atoms.

Here we discuss an experimental scheme in which a beam of Ps atoms in the $2\,^3S_1$ level (henceforth Ps*) may be generated with an energy sufficient to allow SOF measurements of the Ps fine structure to be performed. Such measurements require atoms with energies of several 10's of eV, allowing them to travel cm scale distances during the mean $2P$ lifetime rather than mm, so as to match the waveguide length scales. Most solid-state Ps converters emit low energy Ps atoms, and offer no or limited energy tunability [19]. Some materials do emit more energetic Ps (for example, MgO emits 4 eV Ps [25]), but they generally do so with broad energy and angular distributions [26].

Forward directed Ps beams with higher energies and lower energy spread can, however, be obtained using a gas cell target [27,28], a beam-foil method [29], or a photodetatched Ps ion beam [30,31]. The latter technique is somewhat involved and is not well-suited to the production of excited state Ps beams. The beam foil method has a low efficiency, and it is not known if there is any significant fraction of excited state atoms produced. However, gas cell beam production is relatively straightforward, and has the advantage that, for certain gas targets, a useful fraction of excited state ($n = 2$) atoms will be spontaneously generated [32,33], allowing for the production of a forward directed and energy-tunable Ps* beam. Using Monte Carlo methods, we simulate the properties of such a beam and describe its interaction with two spatially separated waveguides to generate SOF lineshapes for different experimental conditions.

2 Experimental apparatus

A schematic of the proposed experimental setup is shown in Fig. 1. A standard [34] slow positron beam is produced using a ^{22}Na radioactive source with solid neon moderator [35]. Typical conical neon moderators have efficiencies of $\approx$ 0.5%. [36] (NB: higher values that have been reported in the literature probably do not represent long-term beam production). Thus, using a 50 mCi (1.85 GBq) source it is possible to generate positron beams of $\approx 10^7$ s^{-1}. The DC positron beam will be magnetically guided and passed through a gas cell to generate both ground state and excited state Ps atoms [37]. The length of the gas cell and the gas pressure required to optimize Ps* production have been determined by Monte Carlo simulations, as discussed in Sect. 3. Experimentally, Ps* production will be optimized by measuring the beam intensity on a position sensitive multi channel plate (MCP) detector. The MCP will be used to measure both the efficiency of Ps* production and the Ps* beam divergence; the latter can be inferred by measuring the spatial profile of the beam at different distances from the gas cell.

In a magnetic field free region, the Ps* mean lifetime will be 1136 ns [38], which means a 30 eV beam (see below) will travel $\approx$ 261 cm in one lifetime. The experiment therefore requires simultaneous optimization of the beam loss through annihilation, transmission through the waveguides and detection, gas cell pressure/length and the positron beam energy. Moreover,

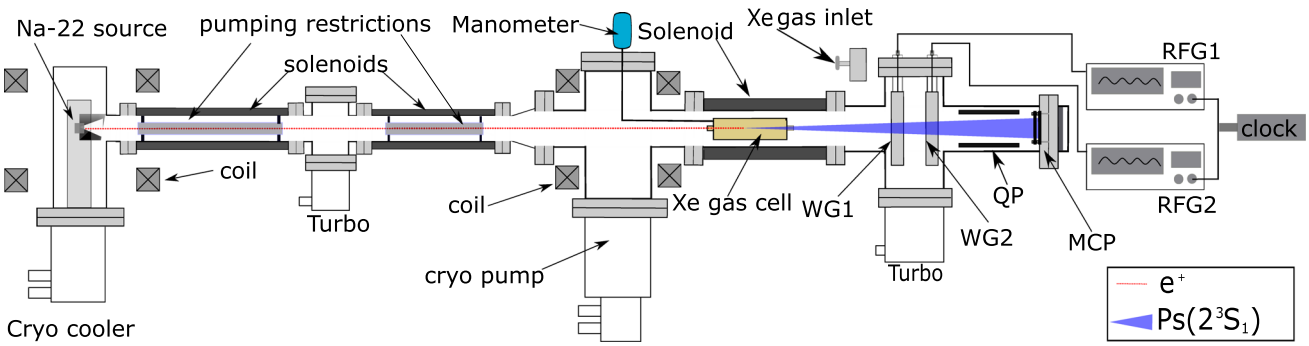

Fig. 1 Schematic of the Ps* beam and waveguide arrangement. Excited state ($2\,^3S_1$) atoms are emitted from the Xe gas cell and subsequently pass through a double waveguide SOF setup. The microwave radiation in the two waveguides (WG1 & WG2) are controlled by two phase-locked signal generators (RFG1 & RFG2), and the transmitted atoms are detected using a microchannel plate detector (MCP) after passing through a set of electric field quenching plates (QP)

ground state atoms will also be produced with almost the same energy as the Ps* beam. Therefore, the system geometry must also take into account the requirement to reduce shorter lived ground state Ps detection (i.e., by using longer path lengths). We note also that, by using mu-metal shielding, we expect to reduce the magnetic field in the measurement region to negligible levels. Ps* detection can be verified and discriminated from Ps, electron, or positron detection in various ways: (1) a transverse magnetic field can be applied to deflect charged particles away from the MCP, (2) an electric field can be applied using a set of quenching plates to induce Ps* to decay (3) the MCP front plate can be biased to reflect charged particles (either positive or negative).

In addition to Ps* beam optimization, it will also be necessary to investigate the conditions for optimal signal generation. The main compromise will be the improved resolution versus the increased loss obtained as the length of the region between the waveguides is increased. Details regarding the expected SOF signal are discussed in Sect. 4, but in general a waveguide separation of several cm will be required. This spacing is a crucial parameter for SOF measurements, and the waveguides will be built so that their separation can be varied *in situ*.

3 Gas cell simulations

Ps beams based on gas cells are useful in that they are energy tuneable over a broad range, as opposed to the relatively slow quasi-monoenergetic emission from solid targets. However, the Ps production in gas cells may be limited by secondary processes such as fragmentation or scattering. In order to optimize the gas cell length and gas pressure, and to estimate the fraction of excited state positronium produced in the experimental apparatus, a Monte Carlo simulation was performed. In this simulation positrons were generated with an energy distribution expected to match the beams produced by neon moderators, i.e., with a variable beam energy and an intrinsic energy spread of ≈ 2 eV full-width-half-max (FWHM) [39]. The beam was modeled considering only the 1-D velocity distribution in the z direction, defined as the positron beam axis. The fraction of Ps* emitted into the forward angles (0 to 6 degrees) was estimated using the calculated differential cross sections of McAlinden and Walters [40]. This data gives the fraction of positronium scattered into the forward angles as 22%. This number was then verified using the experimental data of Shipman et al. [41].

The MC code propagated incident positrons through the gas cell, with a spatial step size $dl = 1$ mm. The probability of generating Ps atoms was determined using the (measured) Ps formation cross section Q_{Ps} [42] for Xenon. The cross section is related to the cell parameters and Ps intensities via the following relationship:

$$Q_{\mathrm{Ps}} = \frac{-1}{n_d l} \ln\left[\frac{I_T}{I_0}\right], \tag{1}$$

where n_d is the number density of the gas, l is the gas cell length, I_T is the transmitted intensity, and I_0 is the initial intensity. This equation was used to determine the probability that a positron entering the cell will form a ground-state Ps atom.

The energy of the produced positronium is given by the relation:

$$E_{\mathrm{Ps}} = E_+ - E_i + \left(\frac{6.8\,\mathrm{eV}}{n^2}\right), \tag{2}$$

where E_+ is the energy of the incoming positron beam, E_i is the ionization threshold of Xenon, and n is the principle quantum number. The ionization threshold for Xenon is 12.13 eV [43].

The probability that a Ps atom was formed in an excited ($n = 2$) state was obtained using Q_{2P}, the cross sections measured by Murtagh et al. [33]. These measurements, shown in Fig. 2a, give the fraction of Q_{2P} formation, relative to the total positronium formation (Q_{Ps}) for all n. The measured data were sensitive to Ps atoms produced in $2P$ states. Assuming that all $n = 2$ Ps states are populated equally in positron-Xenon collisions, the cross section for Ps* formation will be a factor of 4 smaller than Q_{2P}. To give a crude approximation, a 4th-order polynomial fit to Q_{2P} was used to interpolate the cross section to arbitrary positron energies (see Fig. 2a).

Excited state Ps atoms were further propagated through the gas cell with checks for fragmentation. If

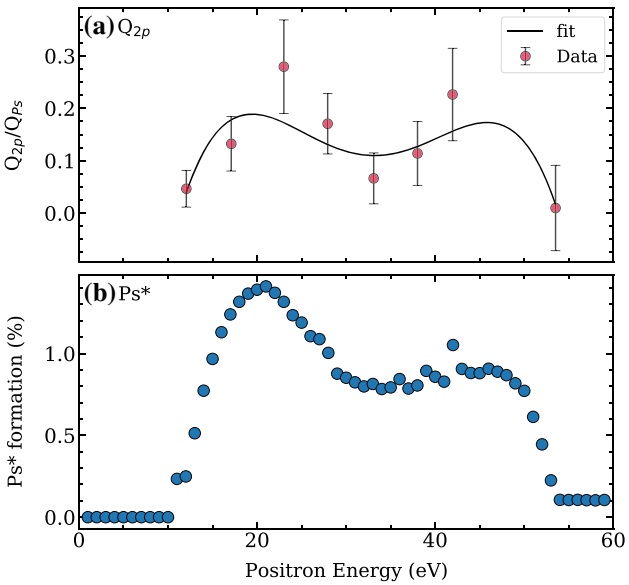

Fig. 2 **a** Measured Q_{2P} data from ref [33] and a polynomial fit (see text for details), expressed as a fraction of the Ps formation cross section Q_{Ps}. **b** Maximum Ps* production efficiencies obtained from simulations with a gas cell pressure of 0 to 6 Pa and a length of 0–15 cm

the Ps* atoms were ionized, then the positron continued through the cell and was checked for further Ps production. Ps fragmentation was determined using calculated ionization cross sections of Starrett et al. [44] These calculations, performed for ground state atoms, show that the Ps fragmentation cross section increases rapidly from 0 eV and peaks around 50 eV, meaning that Ps* beam losses due to fragmentation will increase for higher positron beam energies in the range of interest. Based on geometrical scaling, one can expect this cross section to scale with n^4 [45], meaning that it will be a factor of 16 times larger for Ps*. The calculated ionization cross sections are in agreement with measurements [46] performed in the Ps energy range 18–30 eV.

The total Ps* production efficiency, including Ps fragmentation, is shown in Fig. 2b. This percentage is relative to the sample number of incoming positrons, which was 100,000. These data indicate that useful Ps* production should occur for positron beam energies up to 50 eV.

The optimum gas cell pressure and length were determined from MC simulations performed for positron energies ranging from 0 to 60 eV, pressures ranging from 0 to 6 Pa, and for cell lengths up to 15 cm. The results of these simulations using positron energies of 21 and 40 eV are shown in Fig. 3a, b, respectively. These data show that the optimum Ps* formation can occur over a range where there is a balance of the gas pressure and cell length. That is, a greater cell length allows for more positronium production, but the positronium produced has to travel further to exit the cell, increasing chances of fragmentation. Similarly, a higher gas pressure increases the efficiency of positronium formation but also increases chances of fragmentation. For both of these positron beam energies, the optimum gas cell length and cell pressure were found to be 10 cm and 0.5 Pa. However, there is also good Ps* production for lower cell lengths and higher pressures, for example at 7 cm and 1 Pa for a 21 eV beam. Due to the large error in the experimental data used for this MC, there is a large estimated uncertainty ($> 30\%$ in the MC results).

4 Separated oscillatory field lineshape

The Ps fine structure comprises three intervals $2\,^3S_1 \rightarrow 2\,^3P_J$ $(J = 0, 1, 2)$. For the present discussion, we focus on the transition to $J = 0$ states, which is expected to occur with a transition frequency of 18.49825 GHz [10]. The waveguides used for these measurements are therefore type WR-51, which have dimensions 12.95×6.48 mm [15], meaning that the d dimension described in Fig. 4 is 6.48 mm. The field-free region is a parameter that will need to be optimized experimentally. For the current simulations we use a spacing of $4{\times}d = 25.92$ cm.

A general schematic of the SOF measurement scheme is shown in Fig. 4, in which two waveguides define regions of width d containing an RF-field, and are separated by a field-free region of width D. For a positron beam energy of 40 eV, the mean Ps $n = 2$ energy is 29.6 eV, with a Ps speed of 2.3×10^8 cm/s. Thus the field interaction time is $\tau = 2.8$ ns, and the field free interaction time is $T = 11.4$ ns. The maximum loss of signal due to radiative decay from the $2P$ component of the superposition states will be proportional to $\exp[-\gamma_2(\tau + T)]$. For the parameters above, this amounts to a loss of 98.8% of the signal. Note that this loss rate will be lower for superposition states containing more S character.

In SOF measurements linewidth reduction occurs via two effects, termed interference narrowing and uncertainty-principle narrowing by Fabjan and Pipkin [47]. Interference narrowing arises from the combined effect of the two separated field regions (d) and depends on their relative phase. Uncertainty principle narrowing occurs by selecting longer-lived atoms that are able to traverse the region D.

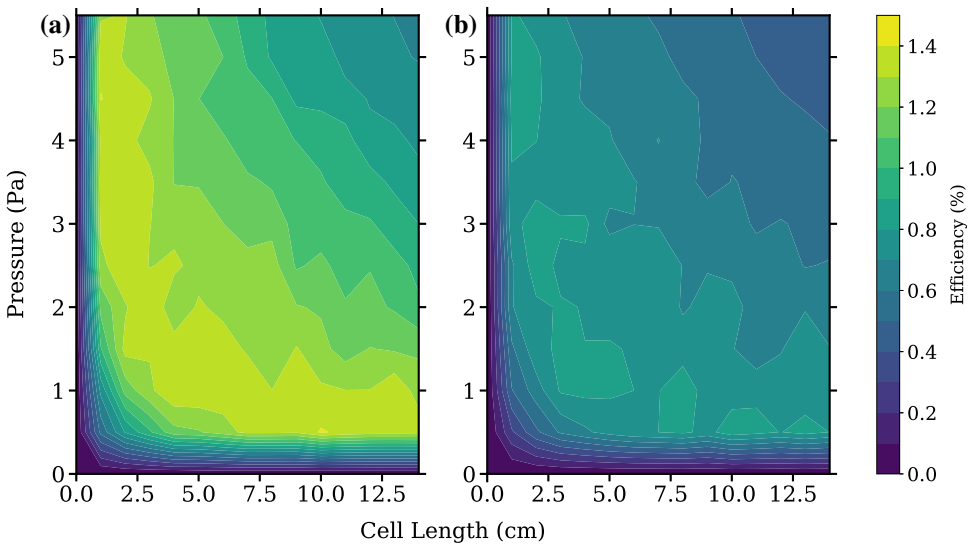

Fig. 3 Ps* production for a positron beam energy of **a** 21 eV, and **b** 40 eV, for different gas cell lengths and pressures. The total number of positron trajectories used in each simulation was 10^5

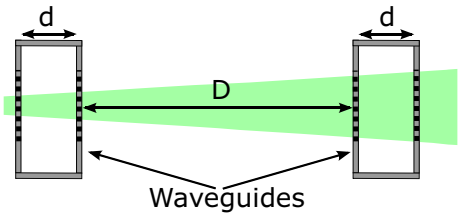

Fig. 4 Schematic representation of the Separated Oscillatory Fields (SOF) setup, showing two waveguides, where an RF field is applied (d), separated by a field free region (D). The (green) cone indicates a diverging beam of Ps* atoms. Ps* is admitted into the waveguide by 95% transmission tungsten mesh

The expected SOF lineshapes were modeled following the treatment of Fabjan and Pipkin [47] in which the system is described by a wave function of the form:

$$|\psi\rangle = c_1(t)\,|1\rangle + c_2(t)\,|2\rangle\,, \tag{3}$$

where $|1\rangle$ corresponds to the $2\,^3S_1$ level and $|2\rangle$ corresponds to the $2\,^3P_0$ level. The decay rate of $|1\rangle$ is $\gamma_1 = 1/1136\,\text{ns}$, the $2\,^3S_1$ annihilation rate. The decay rate of $|2\rangle$ is $\gamma_2 = 1/3.2\,\text{ns}$, which is the $2P$ radiative decay rate.

The amplitudes of the wavefunction after passing through the two separated waveguides are given by equations 19a and 19b in reference [47]:

$$\begin{aligned} c_1(\tau+T+\tau) = \exp\Big[&-\frac{1}{2}(\gamma_1+\gamma_2)\tau \\ &-\frac{1}{2}\gamma_1 T - i(\omega+\omega_1+\omega_2)\tau - i\omega_1 T\Big] \\ &\times\Big[\Big(\cos\frac{1}{2}\alpha\tau + i\cos\theta\sin\frac{1}{2}\alpha\tau\Big)^2 \\ &-\exp\Big[\frac{1}{2}(\gamma_1-\gamma_2)T - i(\delta+\Omega T)\Big] \\ &\sin^2\theta\sin^2\frac{1}{2}\alpha\tau\Big]\,, \end{aligned} \tag{4}$$

$$\begin{aligned} c_2(\tau+T+\tau) = \exp\Big[&-\frac{1}{2}(\gamma_1+\gamma_2)\tau \\ &-\frac{1}{2}\gamma_2 T + i(\omega-\omega_1-\omega_2)\tau - i\omega_2 T\Big] \\ &\times\Big(-i\sin\theta\sin\frac{1}{2}\alpha\tau\Big) \\ &\Big[\Big(\cos\frac{1}{2}\alpha\tau - i\cos\theta\sin\frac{1}{2}\alpha T\Big) \\ &+\exp\Big[\frac{1}{2}(\gamma_2-\gamma_1) + i(\delta+\Omega T)\Big] \\ &\Big(\cos\frac{1}{2}\alpha\tau + i\cos\theta\sin\frac{1}{2}\alpha\tau\Big)\Big]\,, \end{aligned} \tag{5}$$

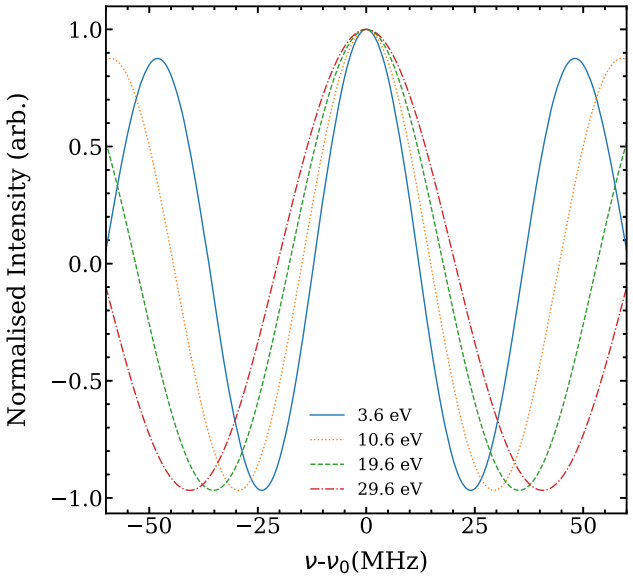

Fig. 5 Normalized SOF lineshapes obtained using Eq. 13 for different Ps* energies as indicated in the legend

where

$$\alpha = [4V^2 + (\Omega + iQ)^2]^{1/2}, \tag{6}$$

$$\omega_0 = \omega_1 - \omega_2, \tag{7}$$

$$\Omega = \omega - \omega_0, \tag{8}$$

$$Q = \frac{1}{2}(\gamma_1 - \gamma_2), \tag{9}$$

$$\sin\theta = 2V/a, \tag{10}$$

$$\cos\theta = (\Omega + iQ)/a, \tag{11}$$

and

$$V = -(1/2\hbar)\,\langle 1|\,\mu_E E_0\,|2\rangle\,, \tag{12}$$

where μ_E is the transition dipole moment and E_0 is the amplitude of the applied RF field, ω_1 and ω_2 are the resonance angular frequencies of the respective sublevels.

These equations describe the evolution of the wavefunction of an atom that traverses two separated oscillatory fields in a time τ, and a field free region in a time T. The first RF field is described by $\bar{E}_0\cos(\omega t)$, and the second field by $\bar{E}_0\cos(\omega t+\delta)$, with oscillating frequency ω, amplitude $\bar{E}$, and phase δ. We assume here that the fields turn on and off instantly and with ideal amplitude profiles. The measurement consists of detecting the surviving Ps* fraction on the MCP detector. This is equivalent to measuring $c_2(\tau+T+\tau)$, and the SOF signal S is then given by the difference of measurements with the fields in and out of phase:

$$S = |c_2(\tau+T+\tau)|^2_{\delta=\pi} - |c_2(\tau+T+\tau)|^2_{\delta=0}. \tag{13}$$

Simulated SOF signals for different Ps* energies are shown in Fig. 5. This signal is normalized and applies to any arbitrary microwave power as long as there is no

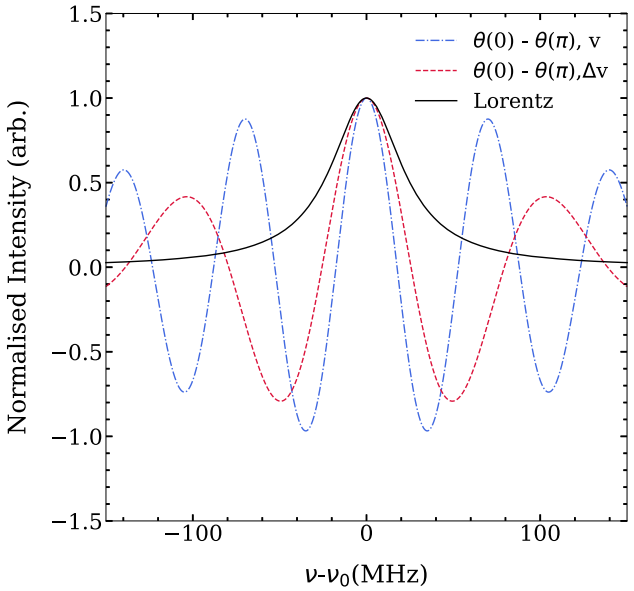

Fig. 6 Normalized SOF lineshapes for a 29.6 eV positronium beam with no velocity spread (blue dash dotted line) and with a 2 eV FWHM velocity spread (dashed red line). The solid black line is a Lorentzian lineshape with a 50 MHz width (FWHM)

significant power broadening. In this figure, the center peak occurs at the resonant frequency $\nu_0 = 18\,498.25$ MHz. This peak is narrower than the single excitation lineshape owing to the interference term that results from Eq. 13, as well as the selection for longer lived atoms. Thus, the centre peak width is determined by the interaction time within the field free regions (T) [47]. Lower energy positronium beams will take longer to traverse the field, and will therefore exhibit narrower linewidths, although this comes at the cost of signal intensity.

In a real experiment, the positron (and hence also the positronium) beam, will have some spread in energies. Using a neon moderator, this is expected to be ≈ 2 eV [16]. An example of variations in the signal arising from this is shown in Fig. 6. A Ps* velocity spread will result in a corresponding spread of field interaction times which broadens the signal. It can be seen from Fig. 6 that, while the linewidth is increased a SOF signal is still present. This is compared to a Lorentzian with linewidth 50 MHz (representing the best-case lineshape expected from a single-field measurement of the $2^3S_1 \rightarrow 2^3P_0$ interval [15]). These data indicate that even after taking into account the beam velocity spread, the SOF measurement still offers a significant improvement in linewidth.

5 Discussion and conclusions

We have shown via simulations that a beam of Ps* atoms (i.e., atoms in the 2^3S_1 level), suitable for performing Ramsey SOF measurements can be produced using a gas cell apparatus. For a positron beam energy of 40 eV, the optimum value for the gas cell length was found to be 10 cm, with a Xenon gas pressure of 0.5 Pa. Using these parameters and measured production cross sections [33,42], the Ps* production efficiency was estimated to be 0.9% for a positron beam energy of 40 eV, and concomitant Ps* beam energy on the order of 30 eV. Based on the Ps* production cross sections, a higher production efficiency is expected at lower energies, but the overall SOF count rates benefit from higher Ps* energies.

Energetic Ps beams produced using gas cells have not been previously used for spectroscopic measurements, which generally require slow atoms to minimize Doppler effects, transit-time broadening and various other unwanted effects [19]. However, for SOF measurements many of these effects are not significant. Moreover, for measurements conducted with short-lived superposition states, fast atoms are essential so as to allow atoms to travel between different spatially separated regions before they decay. We note that this is not only a problem related to Ps experimentation: 30 eV Ps atoms have a speed of $\approx 2.3 \times 10^8$ cm/s, which is comparable to the 3.2×10^8 cm/s hydrogen atoms recently used in a Lamb-shift measurement based on a SOF variant [48] (frequency offset separated oscillatory fields (FOSOF) [49]).

In the SOF measurements described in Sect. 4, Ps* atoms are expected to pass through two waveguides with an average loss fraction of 98.8%. Therefore, for an incident positron beam intensity of 5×10^6 s^{-1} we can expect an overall count rate on the order of 50 Hz. This takes into account 78% loss through beam collimation. The detection efficiency was estimated to be 50% for a MCP [50]).

If successful, the SOF measurements we have described here could be extended to more advanced FOSOF measurements [49]. Rather than measuring lineshapes directly, the FOSOF technique relies on a frequency offset between the separated SOF fields, leading to a continuous phase shift between the two fields. The resulting SOF interference signal then also includes an additional oscillating component that depends on the applied offset frequency. Comparing this signal with the applied offset signal allows the atomic resonance frequency to be determined via a straight line fit, removing any need to fit a (possibly inadequate) function to the full spectral lineshape. Thus, the measurement is not sensitive to the complete frequency response of the system, because it depends on the phase of the signal rather than its amplitude. Since variations in the frequency response seem to be the limiting factor of our previous Ps experiments [22], this would represent a significant advantage for improved Ps $n = 2$ fine structure measurements.

Acknowledgements This work was supported by the EPSRC under Grant No. EP/S036571/1. We are grateful to D. J. Murtagh for useful discussions.

Author contributions

T. J. Babij and D. B. Cassidy discussed the concept and wrote the manuscript. T. J. Babij performed the simulations.

Data Availability Statement This manuscript has no associated data or the data will not be deposited. [Authors' comment: The datasets generated during and/or analyzed during the current study are available from the corresponding author on reasonable request. Email: t.babij@ucl.ac.uk].

References

1. J.A. Wheeler, Polyelectrons. Ann. N. Y. Acad. Sci. **48**(3), 219–238 (1946)
2. S.G. Karshenboim, Precision physics of simple atoms: QED tests, nuclear structure and fundamental constants. Phys. Rep. **422**, 1–63 (2005)
3. S.G. Karshenboim, Precision study of positronium: testing bound state QED theory. Int. J. Mod. Phys. A **19**(23), 3879–3896 (2004)
4. W. Bernreuther, O. Nachtmann, Weak interaction effects in positronium. Z. Physik C Particles Fields **11**(3), 235–245 (1981)
5. C. Frugiuele, J. Pérez-Ríos, C. Peset, Current and future perspectives of positronium and muonium spectroscopy as dark sectors probe. Phys. Rev. D **100**, 015010 (2019)
6. M.S. Safronova, D. Budker, D. DeMille, D.F. Jackson Kimball, A. Derevianko, C.W. Clark, Search for new physics with atoms and molecules. Rev. Mod. Phys. **90**, 025008 (2018)
7. K. Pachucki, S.G. Karshenboim, Complete results for positronium energy levels at order $m\alpha^6$. Phys. Rev. Lett. **80**, 2101–2104 (1998)
8. A. Czarnecki, K. Melnikov, A. Yelkhovsky, Positronium hyperfine splitting: analytical value at $o(m\alpha^6)$. Phys. Rev. Lett. **82**, 311–314 (1999)
9. G.S. Adkins, Higher order corrections to positronium energy levels. J. Phys. Conf. Ser. **1138**, 012005 (2018)
10. A. Czarnecki, K. Melnikov, A. Yelkhovsky, Positronium S-state spectrum: analytic results at $o(m\alpha^6)$. Phys. Rev. A **59**, 4316–4330 (1999)
11. A.P. Mills Jr., S. Berko, K.F. Canter, Fine-structure measurement in the first excited state of positronium. Phys. Rev. Lett. **34**, 1541–1544 (1975)
12. S. Hatamian, R.S. Conti, A. Rich, Measurements of the 2^3S_1-2^3P_J $(J = 0, 1, 2)$ fine-structure splittings in positronium. Phys. Rev. Lett. **58**, 1833–1836 (1987)
13. D. Hagena, R. Ley, D. Weil, G. Werth, W. Arnold, H. Schneider, Precise measurement of n =2 positronium fine-structure intervals. Phys. Rev. Lett. **71**, 2887–2890 (1993)
14. L. Gurung, T.J. Babij, S.D. Hogan, D.B. Cassidy, Precision microwave spectroscopy of the positronium $n = 2$ fine structure. Phys. Rev. Lett. **125**, 073002 (2020)
15. L. Gurung, T.J. Babij, J. Pérez-Ríos, S.D. Hogan, D.B. Cassidy, Observation of asymmetric line shapes in precision microwave spectroscopy of the positronium $2^3S_1 \rightarrow 2^3P_J$ $(J = 1, 2)$ fine-structure intervals. Phys. Rev. A **103**, 042805 (2021)
16. B.S. Cooper, A.M. Alonso, A. Deller, T.E. Wall, D.B. Cassidy, A trap-based pulsed positron beam optimised for positronium laser spectroscopy. Rev. Sci. Instrum. **86**(10), 103101 (2015)
17. L. Liszkay, M.F. Barthe, C. Corbel, P. Crivelli, P. Desgardin, M. Etienne, T. Ohdaira, P. Perez, R. Suzuki, V. Valtchev, A. Walcarius, Orthopositronium annihilation and emission in mesostructured thin silica and silicalite-1 films. Appl. Surf. Sci. **255**(1), 187–190 (2008)
18. A.M. Alonso, S.D. Hogan, D.B. Cassidy, Production of 2^3S_1 positronium atoms by single-photon excitation in an electric field. Phys. Rev. A **95**, 033408 (2017)
19. D.B. Cassidy, Experimental progress in positronium laser physics. Eur. Phys. J. D **72**(3), 53 (2018)
20. D.B. Cassidy, P. Crivelli, T.H. Hisakado, L. Liszkay, V.E. Meligne, P. Perez, H.W.K. Tom, A.P. Mills Jr., Positronium cooling in porous silica measured via Doppler spectroscopy. Phys. Rev. A **81**, 012715 (2010)
21. W. Demtröder, *Laser Spectroscopy*, 3rd edn. (Springer, New York, 2003)
22. L.A. Akopyan, T.J. Babij, K. Lakhmanskiy, D.B. Cassidy, A. Matveev, Line-shape modeling in microwave spectroscopy of the positronium $n = 2$ fine-structure intervals. Phys. Rev. A **104**, 062810 (2021)
23. A. Beyer, L. Maisenbacher, A. Matveev, R. Pohl, K. Khabarova, A. Grinin, T. Lamour, D.C. Yost, T.W. Hänsch, N. Kolachevsky, T. Udem, The Rydberg constant and proton size from atomic hydrogen. Science **358**(6359), 79–85 (2017)
24. N.F. Ramsey, A new molecular beam resonance method. Phys. Rev. **76**, 996–996 (1949)
25. P. Sferlazzo, S. Berko, K.F. Canter, Time-of-flight spectroscopy of positronium emission from quartz and magnesium oxide. Phys. Rev. B **35**, 5315–5318 (1987)
26. P.J. Schultz, K.G. Lynn, Interaction of positron beams with surfaces, thin films, and interfaces. Rev. Mod. Phys. **60**, 701–779 (1988)
27. G. Laricchia, S. Armitage, Á. Kövér, D.J. Murtagh, Ionizing collisions by positrons and positronium impact on the inert atoms, in *Advances in Atomic, Molecular, and Optical Physics*, vol. 56, *Advances in Atomic, Molecular, and Optical Physics*, Academic Press, pp. 1 – 47 (2008)
28. J.R. Machacek, S.J. Buckman, J.P. Sullivan, A pulsed positronium beam using a positron buffer gas trap. Rev. Sci. Instrum. **91**(3), 033311 (2020)

29. A.P. Mills, W.S. Crane, Beam-foil production of fast positronium. Phys. Rev. A **31**, 593–597 (1985)
30. Y. Nagashima, Experiments on positronium negative ions. Phys. Rep. **545**(3), 95–123 (2014). (**Experiments on positronium negative ions**)
31. K. Michishio, L. Chiari, F. Tanaka, N. Oshima, Y. Nagashima, A high-quality and energy-tunable positronium beam system employing a trap-based positron beam. Rev. Sci. Instrum. **90**(2), 023305 (2019)
32. G. Laricchia, M. Charlton, G. Clark, T.C. Griffith, Excited state positronium formation in low density gases. Phys. Lett. A **109**(3), 97–100 (1985)
33. D.J. Murtagh, D.A. Cooke, G. Laricchia, Excited-state positronium formation from helium, argon, and xenon. Phys. Rev. Lett. **102**, 133202 (2009)
34. P.G. Coleman, *Positron Beams and Their Applications*, 1st edn. (World Scientific Publishing Co., Singapore, 2000)
35. A.P. Mills Jr., E.M. Gullikson, Solid neon moderator for producing slow positrons. Appl. Phys. Lett. **49**, 1121 (1986)
36. R. Khatri, M. Charlton, P. Sferlazzo, K.G. Lynn, A.P. Mills Jr., L.O. Roellig, Improvement of rare-gas solid moderators by using conical geometry. Appl. Phys. Lett. **57**(22), 2374–2376 (1990)
37. M. Charlton, J.W. Humberston, in *Positron Physics*, 1st edn., Cambridge Monographs on Atomic, Molecular and Chemical Physics—Volume II. Cambridge University Press, Cambridge (2001)
38. M. Deutsch, Three-quantum decay of positronium. Phys. Rev. **83**, 866–867 (1951)
39. R.G. Greaves, C.M. Surko, Solid neon moderator for positron-trapping experiments. Can. J. Phys. **74**(7–8), 445–448 (1996)
40. M.T. McAlinden, H.R.J. Walters, Differential cross sections for elastic scattering and positronium formation for positron collisions with ne, ar, kr and xe. **89**, 407–418
41. M. Shipman, S. Brawley, D.E. Leslie, S. Armitage, G. Laricchia, Production of collimated positronium by positron scattering from co2, n2 and xe. **66**, 96
42. J.R. Machacek, C. Makochekanwa, A.C.L. Jones, P. Caradonna, D.S. Slaughter, R.P. McEachran, J.P. Sullivan, S.J. Buckman, S. Bellm, B. Lohmann, D.V. Fursa, I. Bray, D.W. Mueller, A.D. Stauffer, Low-energy positron interactions with xenon. New J. Phys. **13**(12), 125004 (2011)
43. A. Kramida, Yu. Ralchenko, J. Reader, NIST ASD Team, NIST Atomic Spectra Database (ver. 5.9) [Online] [2022, May 24]. National Institute of Standards and Technology, Gaithersburg, MD (2021). https://physics.nist.gov/asd
44. C. Starrett, M.T. McAlinden, H.R.J. Walters, Fragmentation of positronium with excitation and ionization of the target. Phys. Rev. A **77**, 042505 (2008)
45. B.I. Deutch, M. Charlton, M.H. Holzscheiter, P. Hvelplund, L.V. Jørgensen, H. Knudsen, G. Laricchia, J.P. Merrison, M.R. Poulsen, Antihydrogen synthesis by the reaction of antiprotons with excited state positronium atoms. Hyperfine Interact. **76**(1), 151–161 (1993)
46. S.J. Brawley, G. Laricchia, Fragmentation in positronium collisions with atoms. J. Phys. Conf. Ser. **199**, 012001 (2010)
47. C.W. Fabjan, F.M. Pipkin, Resonance-narrowed-lamb-shift measurement in hydrogen, $n = 3$. Phys. Rev. A **6**, 556–570 (1972)
48. N. Bezginov, T. Valdez, M. Horbatsch, A. Marsman, A.C. Vutha, E.A. Hessels, A measurement of the atomic hydrogen lamb shift and the proton charge radius. Science **365**(6457), 1007–1012 (2019)
49. A.C. Vutha, E.A. Hessels, Frequency-offset separated oscillatory fields. Phys. Rev. A **92**, 052504 (2015)
50. M.P. Seah, Channel electron multipliers: quantitative intensity measurement-efficiency, gain, linearity and bias effects. J. Electron Spectrosc. Relat. Phenom. **50**(1), 137–157 (1990)